Composites Part A 133 (2020) 105853

Contents lists available at ScienceDirect

Composites Part A

journal homepage: www.elsevier.com/locate/compositesa

Mechanical properties of transparent high strength biocomposites from delignified wood veneer

Erik Jungstedt[a,b], Céline Montanari[a], Sören Östlund[b], Lars Berglund[a,*]

[a] KTH Royal Institute of Technology, Department of Fiber and Polymer Technology, Wallenberg Wood Science Center, 100 44 Stockholm, Sweden
[b] KTH Royal Institute of Technology, Department of Solid Mechanics, 100 44 Stockholm, Sweden

ARTICLE INFO

Keywords:
Composite
Optical Properties
Strain-field
Anisotropy

ABSTRACT

Transparent wood (TW) based on delignified birch veneer and thermoplastic poly(methyl methacrylate) (PMMA) is investigated by uniaxial tensile tests and full-field strain analyses based on digital image correlation techniques. TW is considered as a composite of unidirectional fibers (wood veneer) in a matrix (PMMA). Four in-plane elastic constants along the material axes are reported to enable the usage of continuum mechanics and lamination theory. Longitudinal composite strength is as high as 270 MPa at a reinforcement content of only 25 vol%. The failure behavior is interpreted based on strain field development. Strong reinforcement effects were observed from delignified birch veneer. Despite the fragility of delignified veneers, this constituent provides unexpectedly high reinforcement due to the high cellulose content and favorable stress transfer mechanisms.

1. Introduction

Transparent wood is a new type of biocomposite with the potential to combine high optical transmittance with high mechanical properties for use in structural applications [1,2]. It is based on a chemically treated wood template with low lignin content and preserved cellular structure, as in native wood. This porous reinforcement has high cellulose content, and the pore-space is filled by an optically transparent polymer. High optical transmittance can be obtained if the refractive index of the two different phases are similar. Glass fiber reinforced polymers [3] is another example of potentially transparent composites, but transparent wood has particular potential as a more eco-friendly composite, in combination with high specific modulus and strength. Glass fiber reinforced PMMA can have similar transmittance as the corresponding matrix, but refracting index matching and fiber/matrix interface problems need to be addressed [3]. Similar considerations are important for transparent wood composites, based on delignified balsa wood (D-Balsa/PMMA) [2]. If the volume fraction of cellulose reinforcement, v_f, is increased, this also results in increased through-thickness light-scattering. This indicates that a substantial fraction of scattering originates from the cellulosic cell wall. The transmittance of 1.2 mm thick D-Balsa/PMMA composite is 85% to 34.6% at a wood template volume fraction of around 5% to 65%, whereas neat PMMA shows a transmittance of 90% for similar thickness [2].

The directional orthotropic mechanical properties of D-Balsa/PMMA composites were reported in a previous study [4], and is the main subject of the present study. The material axes, longitudinal (L) and transverse directions (T) for a "unidirectional" ply of a wood veneer are defined in Fig. 1, as well as the specimen directions X and Y. For D-Balsa/PMMA composites, a volume fraction of 12% D-Balsa in PMMA matrix results in an elastic modulus in the L-direction of E_L = 4.3 GPa and E_T = 2.4 GPa, an improvement from 2.3 GPa of neat PMMA. The strength in the longitudinal L-direction along the fibers is σ_L^* = 62.5 MPa and in the transverse T-direction to the fibers σ_T^* = 14.6 MPa [4]. The volume fraction of reinforcement, v_f, can be increased from 5% to 19% by compression of a D-Balsa template prior to polymer infiltration [2]. This increases E_L to 3.6 GPa and the longitudinal ultimate strength increases to σ_L^* = 90 MPa. Mechanical properties of transparent wood based on delignified basswood impregnated with epoxy (D-basswood/Epoxy) has also been reported [1]. D-basswood/Epoxy composites showed E_L = 5.78 GPa and σ_L^* = 42.7 MPa, which means higher modulus but lower strength compared with D-Balsa/PMMA at v_f = 19% [2]. Although basswood has a higher relative density [6] than balsa, a different delignification scheme was used and the final v_f of wood reinforcement in D-basswood/Epoxy was not reported.

As with other composites, transparent wood laminates from unidirectional plies (laminae) can be prepared to tailor mechanical performance of the laminate by control of fiber direction of each ply (lamina) [4]. In order to design elastic properties of laminates, four in-

* Corresponding author.
E-mail address: blund@kth.se (L. Berglund).

https://doi.org/10.1016/j.compositesa.2020.105853
Received 26 November 2019; Received in revised form 20 February 2020; Accepted 22 February 2020
Available online 24 February 2020
1359-835X/

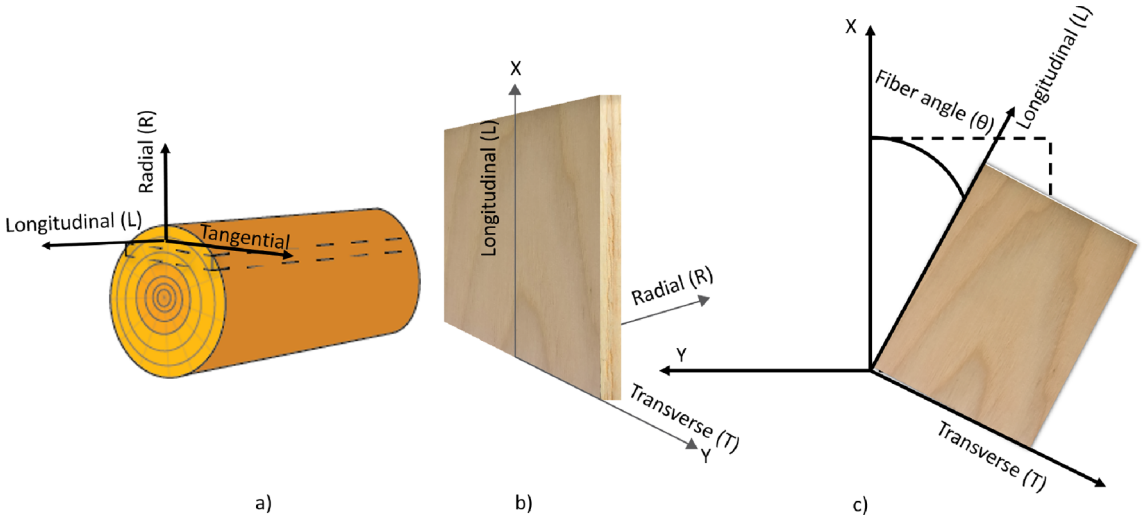

Fig. 1. Material directions in wood, based on specimen position in the tree stem. In (a), the tree stem is anisotropic on a macro scale, but pointwise orthotropic since a tree trunk can be considered as cylindrical with three principal axes: longitudinal (L) fiber direction, tangential and radial (R) [5]. In (b), if a wood veneer is cut so that the material axes, L-axis and tangential axis, coincides with two mutually orthogonal axes for specimen geometry (Y and X), the material can be considered as orthotropic. If the specimen is from the outer perimeter of the tree stem, the tangential axis will coincide with the transverse axis (T). In (c) the wood veneer can be rotated with an angle, θ, from the mutually orthogonal specimen axes Y and X. (For interpretation of the references to colour in this figure legend, the reader is referred to the web version of this article.)

plane elastic parameters of a single ply need to be determined. Full-field displacement measurement techniques are helpful, since strain homogeneity can be investigated in two dimensions. The deformation of a speckled region of interest (ROI) at the surface of the material specimen is analyzed with digital image correlation (DIC). DIC is a non-contact measurement technique, well-suited to determine constitutive properties of heterogenous materials [7]. For wood and wood polymer composites, DIC also allows for measurement of local strains and strain gradients to investigate the failure process [8]. For cross-laminated timber, DIC has been used for qualitative measurements to predict and locate the failure modes and regions in each lamina [9]. DIC is often used to investigate damage development in heterogeneous materials, and has been used to accurately determine elastic properties of wood in tension [10,11] and/or in compression [12]. For wood, however, the heterogeneity of the strain field in clear wood structures and composites has seldom been investigated in detail. Such studies would improve our understanding of deformation mechanisms in anisotropic wood materials.

For the purpose of general understanding of mechanical wood properties, microscale deformation mechanisms of native balsa wood have been studied by in-situ microscopy under different loading conditions and related to the mechanical properties of the solid wood cell wall [13]. DIC was also used on a slightly larger length-scale to measure the local softwood stiffness differences between earlywood and latewood [14]. Gibson and Ashby [13] provide a set of micromechanics models for different moduli of wood, as well as failure criteria for basic modes of failure. The most important microstructural parameter is relative density, which can also be expressed as the volume fraction of solid tissue. As an example, the longitudinal modulus of wood (in the fiber direction) is simply given by the cell wall modulus, $E_{fl,}$ multiplied by the volume fraction of the cell wall. For a basswood/polymer composite [15] with pore space filled by a thermoplastic, a simple rule of mixtures approach was used where the polymer contribution was included, and experimental data were predicted successfully. This type of analysis has not been performed for the case of composites based on delignified wood templates. Possibly, reinforcement effects and the role of lignin can be analyzed in this way.

The main material of interest here is a D-Birch/PMMA composite based on *Betula Pendula*. In the context of transparent wood, birch is a hardwood species of high density. The four in-plane elastic parameters of a single, unidirectional ply composite will be determined, and DIC is used to investigate the deformation field on the surface of the wood/polymer biocomposites. Three different deformation controlled tensile tests are used to determine the four elastic constitutive parameters; one test in each in-plane material direction and one off-axis test to determine the shear modulus, G_{LT} [16]. The ultimate strengths and strains to failure are measured in the tests, and the corresponding strain fields are analyzed. The effects of solid polymer in the wood pore space on mechanical properties and strain field details are also investigated. The main engineering science objective is to evaluate the contribution of the delignified template to mechanical properties, and to investigate the role of the polymer matrix for mechanical properties and deformation mechanisms. Surprisingly strong reinforcement effects are found, and the reasons for this are discussed.

2. Materials and methods

2.1. Material components and composite processing

The D-Birch/PMMA composite is based on thin birch veneer, which was first delignified, then impregnated by pre-polymerized methyl methacrylate, MMA, followed by polymerization as illustrated in Fig. 2. The optical transparency of the composite in Fig. 2 is obtained by chemical removal of lignin chromophores and subsequent filling of the porous lumen space with PMMA of matching refractive index with the cellulosic cell wall of wood. The Birch/PMMA was similarly prepared but without the delignification step.

The birch species (*Betula Pendula*) was grown in Nordic climate, purchased from Fredricson Trä AB. To prepare specimens where material directions coincide with specimen directions, thin veneers of 0.5 mm were plain sawn from the outer region of the stem where the growth ring curvature was small. The veneers were delignified by using 1 wt% of sodium chlorite ($NaClO_2$, Alfa Aesar) with an acetate buffer solution (pH 4.6) at 80 °C [2]. The MMA (Sigma-Aldrich) was pre-polymerized with 0.3 wt% of the initiator 2,2′-azobis (2- methylpropionitrile) (Sigma-Aldrich) in a round-bottom flask for 17 min at 70 °C [2]. Both the birch and D-Birch templates were washed sequentially in water, ethanol, acetone and then placed in baths of PMMA precursors, separately, for vacuum infiltration during 2–3 days. Both impregnated templates were packaged between two glass slides, wrapped with

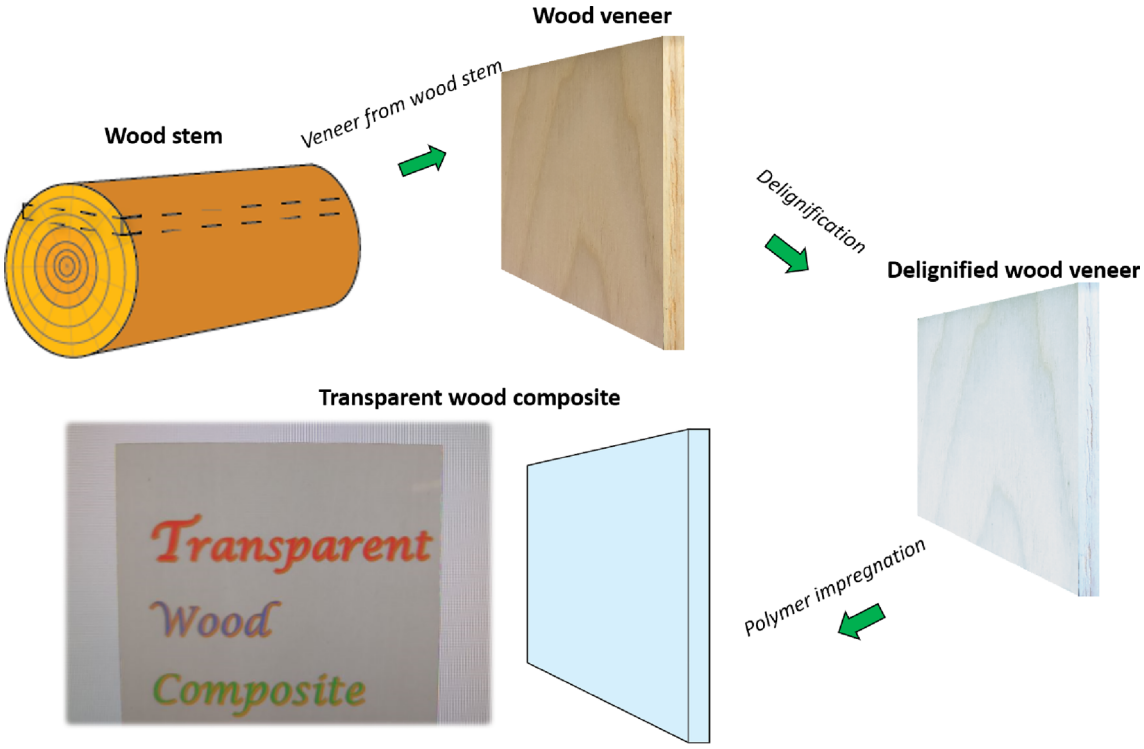

Fig. 2. Schematic illustration of transparent wood composites preparation, and the resulting appearance of the transparent wood composite. A thin veneer was cut from a birch stem and delignified. The resulting white birch template was then impregnated with a methyl methacrylate polymer precursor, followed by polymerization so that the transparent wood composite was formed. (For interpretation of the references to colour in this figure legend, the reader is referred to the web version of this article.)

aluminum foil and then placed in an oven at 45 °C for one day and then increased to 70 °C, for additionally one day.

The lignin content of birch and D-Birch was determined by a Klason lignin tests in accordance to the TAPPI T 222 om-2 method [17]. The content of hemicellulose and cellulose was determined by carbohydrate analysis using a Dionex ICS-3000 ion chromatography system (Thermo Fisher Scientific, USA). Arabinose, galactose, xylose, mannose and glucose are the main monosaccharides of birch [18], where all the glucose was assume to be cellulose.

For birch and D-Birch density estimates, the weight was measured on oven-dried (105 °C) samples. It was assumed that the cell wall density, ρ_s, was 1500 kg/m^3 both for D-Birch and birch. The density of PMMA, ρ_m, was measured. The weight fraction, w_f, of D-Birch was estimated based on weight loss from delignification, measured on freeze-dried samples. The weight fraction, w_m, of PMMA was estimated by subtraction of the known D-birch weight from the total weight of the composite. The volume fractions of the components were based on weight fractions and the densities of each constituent.

The cross-sections of the materials were prepared using an ultramicrotome (RMC PowerTome MT-XL, UK). The samples were Pt/Pd sputtered for 5 s using a Cressington 208 HR sputter Coater. The microstructures were analyzed using a field-emission scanning electron microscope (Hitachi SEM S-4800, Japan).

Optical transmittance was measured using an integrating sphere and a quartz tungsten halogen light source (model 66181, Oriel Instruments) as incident beam for stable and strong output within the visible and near infrared region (400–800 nm). Transmittance was measured and haze was calculated in accordance to ASTM D1003-13 [19].

2.2. Strain analysis

A subset-based method of Digital Image Correlation (DIC) was used to post-process sequential images from the mechanical tests. Full field strain plots were obtained by the DIC analysis. The average strain of the strain field was used for stress-strain plots. One camera was used for 2D analysis and the out-of-plane motion was neglected by using a telecentric lens [20]. A telecentric lens, with a field of view of 61.4 × 51.5 mm^2, was mounted to a 5 Mpixel LIMESS CCD (2/3″ 8-bit sensor) camera. The camera was mounted a distance of around 250 mm to the object. The length to pixel ratio was around 0.03 mm/pixel and images were captured every 200 ms with a shutter speed of 11 ms. For strain plots on D-Birch/PMMA and Birch/PMMA the subset size was set to around 31–37 pixels, with a speckled region of more than 3 features [21], and a step size of 13–15 pixels and a strain window of 11–15 pixels (average filter). For wood, the subset size was set to 49–51 and step size to 13–15 was kept, to have similar noise floor. The resultant strain and displacement noise floor were around 0.1 μm/mm and 0.2 μm, respectively.

The speckle pattern was made by applying black acrylic matt paint on the surface coating in the region of interest (ROI). Two light sources from either side of the camera was used to ensure well-distributed light, and sufficient contrast. The DIC was performed using GOM Software (Rev. 115656, Build 2019-02-15) with a bi-cubic interpolation function and incremental correlation. The strain measures were engineering strains to be consistent with engineering stresses. Poisson's ratio, ν_{LT}, was affected by the resolution, since the lateral strain in the small strain regions was highly affected by the noise floor. Therefore, ν_{LT} was only measured between strains $1{\cdot}10^{-3}$ to $3{\cdot}10^{-3}$.

2.3. Mechanical testing

Two elastic moduli, E_L and E_T, were determined by tensile tests with the loading direction aligned with the principal axes L and T. Poisson's ratio, ν_{LT}, was determined by the negative ratio of strain in the direction of the L- and T-axes, while loaded in the L-direction. Samples were typically 100–110 mm long with a width of 10 mm, and the tensile grip distance were 50 mm. Birch/PMMA and D-Birch/PMMA samples had a

thickness of around 0.65 mm. The birch samples were conditioned so that they had a moisture content of 10%.

The tests were carried out in an environment-controlled room with temperature of 22 °C and relative humidity of 50%. The tensile tests were performed on a universal testing machine (Instron 5566, UK), equipped with a 10 kN load cell and screw side action grips. The piston speed was set to 5 mm/min to have the same strain rate as previous work on similar materials [2,4]. Elastic moduli, E_L and E_T, was determined within the strain interval $5{\cdot}10^{-4}$ to $2{\cdot}10^{-3}$.

The off-axis shear test was designed by tensile tests of strip geometries where the fiber directions were inclined at an angle, θ, to the loading axis [22]. One design was based on 10° off-axis fiber angle [16]. Additional tests were made with a 45° off-axis fiber angle, for comparison. Shear stress and strains were projected to the material axes to determine the shear modulus, G_{LT}, which was determined as the ratio of shear strain, $2\varepsilon_{LT}$, and shear stress σ_{LT}. Both variables $2\varepsilon_{LT}$ and σ_{LT} along the material axes was determined from

$$2\varepsilon_{LT} = (\varepsilon_y - \varepsilon_x)\sin(2\theta) + \varepsilon_{xy}\cos(2\theta) \quad (1)$$

$$\sigma_{LT} = \frac{(\sigma_y - \sigma_x)}{2}\sin(2\theta) + \sigma_{xy}\cos(2\theta) \quad (2)$$

The average strain components ε_y, ε_x and ε_{xy} are determined from the DIC analysis, along the tensile test axis y and x. The nominal stress component σ_x was measured from the load cell, and the remainder σ_{xy} and σ_y were assumed to be zero.

Birch and D-Birch/PMMA specimens with fibers 10° off-axis were cut to 102 × 8.5 mm^2, and specimens with fibers 45° off-axis were cut to 140 × 8.5 mm^2. For practical reasons related to annual ring curvature, it was not possible to fulfill the specimen dimension requirements [16]. The piston speed, of the testing machine, was set to 5 mm/min with a tensile grip gap of 50 mm. The average shear strain for determining G_{LT} was chosen from $5{\cdot}10^{-4}$ to $2{\cdot}10^{-3}$ as the shear strain field from the DIC analysis was sufficiently homogeneous within this region.

3. Results and discussion

3.1. Processing and microstructure

The process for delignified D-Birch/PMMA preparation is illustrated in Fig. 2. There are obvious similarities with vacuum impregnation processes for polymeric fiber composites. D-Birch or the birch reference were soaked in acetone, to facilitate impregnation by the reactive MMA polymer precursor. Acetone was evaporated during the process and MMA was polymerized into PMMA polymer. The microstructures of birch and the resulting transparent wood composites are presented in Fig. 3(a), (b), (d) and (e). The cellular structures of birch and D-Birch veneer are apparent in Fig. 3(a) and (e). The large pores are vessels for water transport and the smaller ones are lumen space in the fiber cells. In birch, supporting fiber cells occupy about 65–70% of the volume, and the vessels about 25%. Fig. 3(a), (b) and (e) show transparent wood composites with PMMA present in the pore space. No polymer is expected in the wood cell wall, since there is no apparent cell wall swelling. The images of the composites also support low void content. The optical transmittance of the final D-Birch/PMMA composite was quite high, 70% for a 1.3 mm thick sample; see Fig. 3(c). The high optical transmittance indicates uniform PMMA distribution and that the porosity in the transparent D-Birch/PMMA composite is very limited. Optical haze, which is the ratio of forward scattered transmittance over total transmitted light, was around 70% for a 1.3 mm thick D-Birch/PMMA, Fig. 3(f). The high haze is comparable with previous report on D-Balsa/PMMA [2] and provides diffused light, of interest in some interior design applications.

In a composite materials context, the composition, structure and volume fraction of the D-Birch reinforcement phase are important. In Table 1, the chemical composition before and after delignification is shown. Initially, the birch cell wall contains cellulose fibrils, in a matrix of hemicellulose and lignin biopolymers. Most of the lignin was removed by delignification so that the D-Birch contained mainly hemicellulose and cellulose.

The average weight loss was 25%, which is similar to previously reported [23]. Most of the middle lamella between birch cells is removed during delignification [2]. Delignification increases micro and nanoscale porosity in the wood cell wall, but also increases the high-modulus cellulose fibril content from 50 to about 70 wt%, see Table 1. Density results verify that porosity increases when lignin is removed, see density data for freeze-dried D-Birch in Table 2. Data are also provided for Birch/PMMA composites, which are not delignified.

The volume fractions of birch reinforcement, v_f, are also reported in Table 2. Indeed, the birch volume fraction is lower for the D-Birch. Possibly, the reason is that delignification induces additional porosity. The wood volume fractions in the composites are lower than for the neat birch substrates (birch and D-Birch), since the composites have a layer of PMMA at the surface.

3.2. Elastic properties and strain field analysis

3.2.1. Longitudinal modulus E_L and Poisson's ratio ν_{LT}

Elastic properties can be used to describe the behavior of transparent wood lamellae and by the use of classical laminate plate theory also for plywood laminates [5]. The properties E_L and ν_{LT} were determined in a uniaxial tensile test, where the strain field was determined by DIC. Data are presented in Table 2. Note that the mechanical properties of D-Birch cannot be tested, since removal of lignin severely degrades the mechanical integrity of the material. Lignin acts as a micro/nanoscale binder in the birch cell wall. The typical stress-strain curves for transparent wood composites are presented in Fig. 4(a). The stress-strain behavior is linear, with catastrophic final fracture at the maximum stress. Viscoelastic or viscoplastic effects from the PMMA matrix appear not to be important in the experiment. The neat birch showed an E_L of 16.4 GPa at a birch volume fraction of 0.41, see Table 2, which is higher than data reported by Dinwoodie [6]. The cellulose microfibril angle (MFA) in the birch cell wall may be smaller in the present material. This parameter varies with the location in the tree [24]. The longitudinal modulus, E_L, of D-Birch/PMMA is 19.3 GPa, which is higher than for neat birch (≈16.4 GPa). The reason is the stiffness contribution from the PMMA polymer. The Birch/PMMA composite has an E_L of 15.3 GPa, which is lower than for D-Birch/PMMA, although the wood volume fraction, v_f, is higher in Birch/PMMA. It means that the effective modulus of the D-Birch reinforcement is higher than for neat birch.

The average Poisson's ratio, ν_{LT}, for D-Birch/PMMA was 0.38. For neat birch, the average ν_{LT} was 0.48, which is close to the values reported in Dinwoodie [6]. Most likely, the presence of polymer in the pore space is reducing lateral contraction during loading.

3.2.2. Transverse modulus E_T

Composite material structures are subjected to multiaxial loads, which means that the transverse properties are important due to their low values; see Fig. 4(b) and Table 3. Neat birch shows the lowest E_T and the lowest transverse strength, σ_T^*. The biocomposites (Birch/PMMA and D-Birch/PMMA) show higher E_T and transverse strength than the neat birch wood reference, but are very brittle with low strain to failure. Note that strength and strain to failure in transverse tension are even inferior to properties of neat PMMA. E_T is much lower than E_L and may limit the performance of a structural component in which the material is used. The transverse modulus, E_T, for neat birch is lower than for transparent wood composites, since the main deformation mechanism is cell wall bending at the scale of individual wood cells [13]. As the wood lumen is filled with PMMA, the cell wall bending mechanism is constrained and E_T is consequently increased.

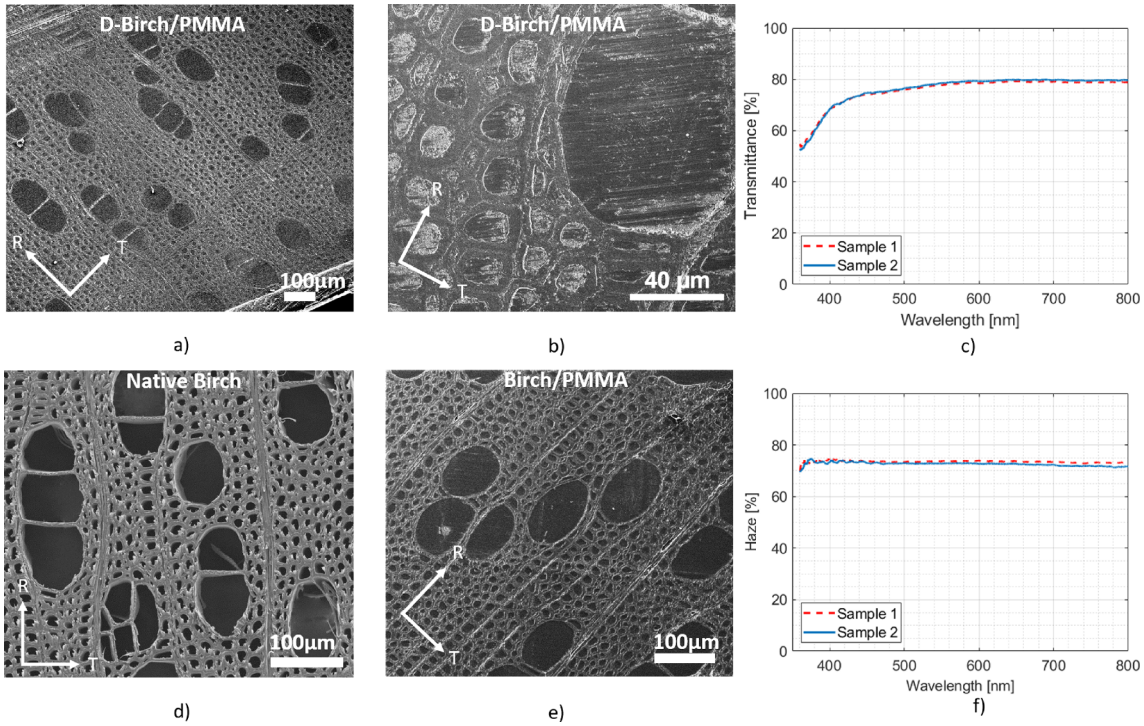

Fig. 3. SEM images of the microstructure of D-Birch/PMMA, Birch/PMMA and neat birch with corresponding radial and transverse (tangential) material directions, and optical measurement data of 1.3 mm thick D-Birch/PMMA specimens. The dark gray regions in the composites are PMMA located in the birch lumen and vessels; (a) and (b): D-Birch/PMMA composites at different magnification; (c) Optical transmittance; (d) neat birch where the dark regions are pores (vessels and fiber lumen space); (e) Birch/PMMA composite; (f) Optical Haze. (For interpretation of the references to colour in this figure legend, the reader is referred to the web version of this article.)

Table 1
Chemical composition of neat birch and delignified birch.

Material	Lignin content [%]	Hemicellulose content [%]	Cellulose [%]
Birch	19.8	30.0	50.0
D-Birch	2.8	26.7	70.5

3.2.3. In-plane shear modulus

An off -axis tensile test was used to determine the G_{LT}, since G_{LT} is required in the laminate plate theory for laminates from transparent wood composites [4]. The off-axis test has been used for unidirectional fiber composites [16], and can be adapted for wood [25,26]. The analysis is presented in the Materials and Methods section. Typical stress-strain curves are presented in Fig. 4(c) and G_{LT} data in Table 2. One may note that the values for G_{LT} are quite low. Two off-axis angles were used (10° and 45°), and the small strain values for G_{LT} were very similar for both angles. The ultimate strength was higher for $\theta = 10°$, however, values of ultimate shear strength, σ^*_{LT}, are not reliable for the present test method due to shear coupling effects [27]. The shear modulus, $G_{LT,}$ for D-Birch/PMMA is substantially higher than for neat birch. Again, the polymer phase constrains the cell wall bending mechanisms [13].

3.2.4. Off-axis orientation effects on composite modulus E_θ

Based on the four in-plane elastic constants, the composite modulus, E_θ, for a unidirectional lamina loaded at an off-axis angle θ is given by:

$$E_\theta = \left(\frac{\cos^4\theta}{E_L} + \frac{\sin^4\theta}{E_T} + \left(\frac{1}{G_{LT}} - \frac{2\nu_{LT}}{E_L} \right) \sin^2\theta\cos^2\theta \right)^{-1} \quad (3)$$

Data for the four elastic constants E_L, E_T, G_{LT} and ν_{LT} in Table 2 are used and predictions for E_θ, as a function of θ, are presented in Fig. 4(d). The anisotropy ratio E_L/E_T is lower for D-Birch/PMMA compared with neat birch, since the polymer phase increases E_θ at larger off-axis angles. Experimental data from D-Birch/PMMA for $\theta = 10°$ and 45° are provided in Fig. 4(d), and are in reasonable agreement with predictions.

Table 2
Material properties and volume fraction of wood component. Note that neat birch and D-Birch are porous materials, so that the remaining volume of the material is air.

Material	Birch	D-Birch	Birch/PMMA	D-Birch/PMMA	PMMA
E_L [GPa]	16.4 ± 1.0		15.3 ± 0.5	19.3 ± 0.6	
E_T [GPa]	0.5 ± 0.0		3.3 ± 0.2	3.4 ± 0.2	
E_m [GPa]					2.4 ± 0.3
G_{LT} [GPa]	0.8 ± 0.1			1.3 ± 0.2	
ν_{LT}	0.48 ± 0.0		0.44 ± 0.0	0.38 ± 0.0	0.35
Density [kg/m^3]	610* ± 7	456* ± 18	1248 ± 6	1215 ± 5	1113 ± 17
v_f	0.41	0.30	0.28	0.25	

* Oven-dry density.

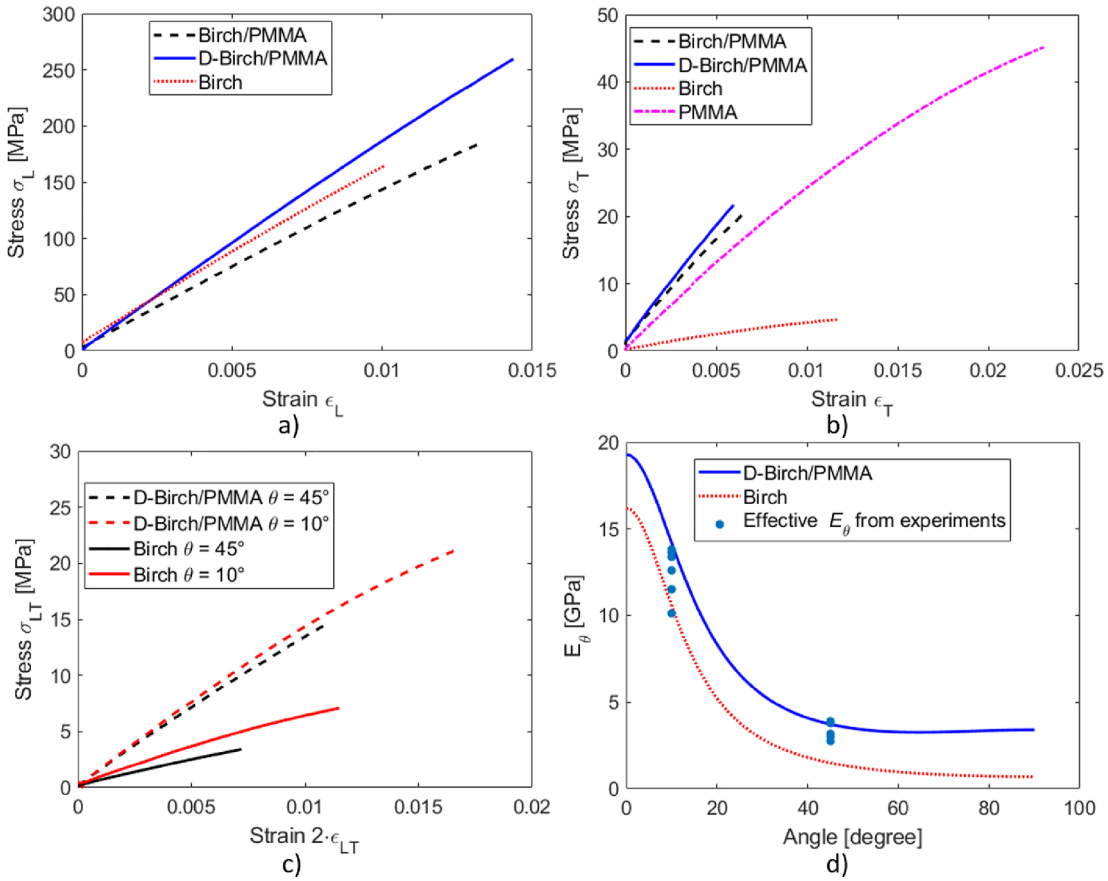

Fig. 4. Typical stress-strain curves of neat birch, D-Birch/PMMA, Birch/PMMA and PMMA; (a) longitudinal tensile test; (b) transverse tensile test (tangential); (c) off-axis shear test with results reported in the material axes; (d) Effective composite modulus E_θ as a function of fiber angle including experimental results from D-Birch/PMMA. (For interpretation of the references to colour in this figure legend, the reader is referred to the web version of this article.)

3.3. Strain field development and failure

3.3.1. Longitudinal tensile loading

The strain field development is used to investigate the deformation mechanisms. Data for neat birch, Birch/PMMA and D-birch/PMMA are presented in Fig. 5 (note that the color-coded strain scales differ between different materials). The corresponding principal strain curves are presented in Fig. 5(a). In D-Birch/PMMA, strain field inhomogeneities start to develop already at an average strain of $0.2{\cdot}10^{-2}$, see Fig. 5(c). Distinct regions of locally increased strain are formed in the lower right region of the specimen. For neat birch, Fig. 5(d), the local strain gradients are much higher. Possibly the reason is larger differences in local stiffness at the scale of millimeters for a porous material such as birch. In PMMA matrix composites, such differences are smaller due to the polymer phase. Neat birch shows a band of increased strain, ε_L, see Fig. 5(d), but this does not occur for the biocomposites (Birch/PMMA and D-Birch/PMMA). Inhomogeneities in neat birch may be in the form of local density differences. We are not aware of previous discussions of shear strain, ε_{LT}, in longitudinal tension specimens of wood; see Fig. 5(a). Possibly, the reason for local shear strain is in local stiffness inhomogeneities, which may be caused by the annual ring structure.

At ultimate fracture of birch, vertical cracks are formed parallel to the fiber direction; see Fig. 5(d). This splintering type of failure in tension has been discussed previously, mostly for softwoods [5,6] and to some extent for hardwoods [28], where the phenomenon is interpreted at the fiber cell wall scale. It seems that vertical cracks in "splintering" failure are formed at fiber fracture. It is then possible that the low transverse strength and toughness of wood contributes to the phenomenon during dynamic crack growth. The fracture toughness is much lower for vertical direction crack growth so that subsequent fiber fractures are combined with vertical cracking. This fracture mechanism also takes place during longitudinal fracture of unidirectional fiber/polymer matrix composites [29]. D-Birch/PMMA also showed crack splintering, possibly due to a weak crack-path along delignified cell walls, whereas Birch/PMMA showed horizontal crack growth fracture see Fig. 5(e)–(f); perhaps the presence of lignin in the cell wall increases vertical crack growth resistance. Note that the fracture surface shows a comparably flat surface at the scale of a few hundred micrometers (Fig. 5(b)). The lack of extensive wood cell wall pull-out may indicate

Table 3
Ultimate strength and strain to failure.

Material	σ_L^*[MPa]	ε_L^*[%]	σ_T^*[MPa]	ε_T^*[%]	σ_{LT}^*[MPa]
Birch (v_f = 0.41)	166.8 ± 16.4	0.9 ± 1.4	4.2 ± 0.6	1.0 ± 0.2	
PMMA	43.4 ± 8.4	2.3 ± 0.6			
D-Birch/PMMA (v_f = 0.25)	262.7 ± 16.4	1.4 ± 0.1	21.1 ± 1.9	0.7 ± 0.0	19.0 ± 4.5
Birch/PMMA (v_f = 0.28)	192.7 ± 14.4	1.3 ± 0.1	20.4 ± 0.9	0.7 ± 0.0	

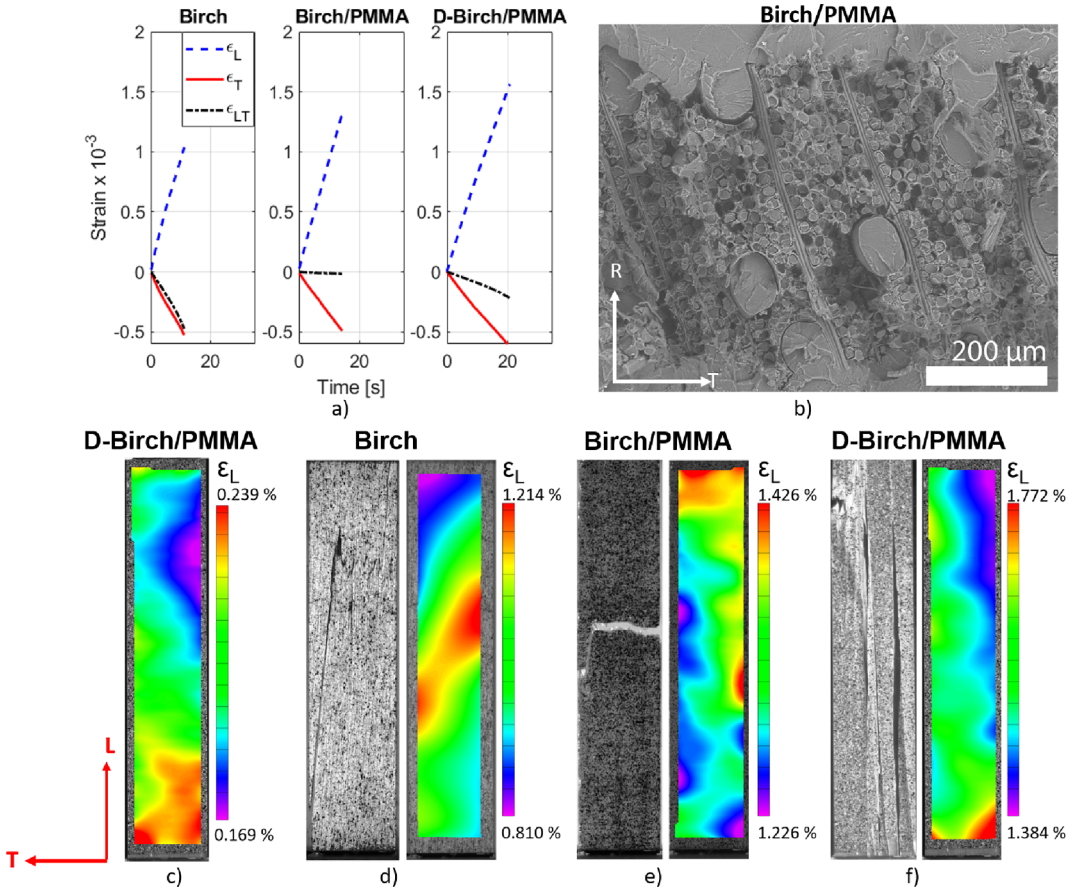

Fig. 5. Strain field maps and plots at different average strain levels for longitudinal tension specimen (L-direction is vertical) and corresponding failed specimen and fracture surface; (a) Average strain plots for all materials; (b) Fracture surface of Birch/PMMA; (c) D-birch/PMMA in low strain region (0.2%); (d) Neat birch; (e) Birch/PMMA; (f) D-Birch/PMMA. Note that the color-coded strain scales differ between different materials. (For interpretation of the references to colour in this figure legend, the reader is referred to the web version of this article.)

favorable Birch/PMMA interfacial toughness. For both D-Birch/PMMA and Birch/PMMA composites fracture appears to initiate from the specimen edge where microcracks from specimen preparation are present.

Strength data are reported in Table 3, and the stress-strain curves in Fig. 1(a). Note that strength values from small specimens of neat birch depend on details of microstructural variation (e.g. density variation in annual rings) and are not valid for engineering design of large structures. There is a large difference in σ_L^* between birch (167 MPa at $v_f = 0.41$) Birch/PMMA (193 MPa at $v_f = 0.28$) and D-Birch/PMMA (263 MPa at $v_f = 0.25$). Lignin has been removed from the cell wall of D-Birch/PMMA and the effective D-Birch modulus may increase by the higher cellulose volume fraction in the cell wall. Although the material differences in E_L determined at small strains are not so large, there are substantial stress level differences at larger strains in Fig. 4. The D-Birch provides better reinforcement at higher strains and shows larger strain to failure. The delignified D-Birch reinforcement combined with PMMA may show more favorable subcritical failure mechanisms. One may speculate that the small-scale distribution of PMMA is more favorable for D-Birch/PMMA.

3.3.2. Transverse tension

Stress-strain curves in transverse tension have already been discussed, Fig. 4, although the deformation mechanisms need further analysis. The final crack growth is parallel to the fiber direction, where crack growth toughness is low. Strain fields in the low strain region and close to failure are presented in Fig. 6. For D-Birch/PMMA, some strain localization takes place in the middle section of the specimen already at an average strain, ε_T, of $2{\cdot}10^{-3}$. Just prior to fracture, localization is more severe, see Fig. 6(d), and the specimen separates into two parts by sudden crack growth. The strain field close to final fracture is much more homogeneous for the biocomposites (D-Birch/PMMA, Birch/PMMA) compared to the neat birch, see Fig. 6(b)–(d). Large strain gradients are present in the neat birch, with distinct horizontal strips of high local strain, possibly in the low-density earlywood regions of the annual rings. Deformation in neat birch in transverse tension is related to local cell wall bending [13], which is reduced in D-Birch/PMMA and Birch/PMMA, where the PMMA-phase in the lumen suppresses local cell wall deformation. Fig. 6(e)–(f). indicates that failure is initiated at the ray cells during transverse (tangential) direction loading. Ray cells run in the radial direction of the tree stem and are oriented perpendicular to the transverse loading direction, as defined in the present study, see Fig. 1. Failure in the ray cell region has been discussed previously for wood [5], and the ray cell appears to function as a defect. The fracture surface in Fig. 6(f) for delignified D-Birch/PMMA is slightly more “clean” and flat, compared with Birch/PMMA in Fig. 6(e). This may be due to preferable crack growth in the delignified and weakened middle lamella between cells. In Table 3, one may note that transverse strength, σ_T^*, of neat Birch is only around 4 MPa, whereas σ_T^* reaches around 20 MPa for the biocomposites D-Birch/PMMA and Birch/PMMA. This is an interesting engineering design advantage of polymer impregnated transparent wood biocomposites.

3.3.3. 10° off-axis shear specimens

Strain-fields for two materials are presented in Fig. 7, neat birch and the D-Birch/PMMA composite. Note that the reported strains have the

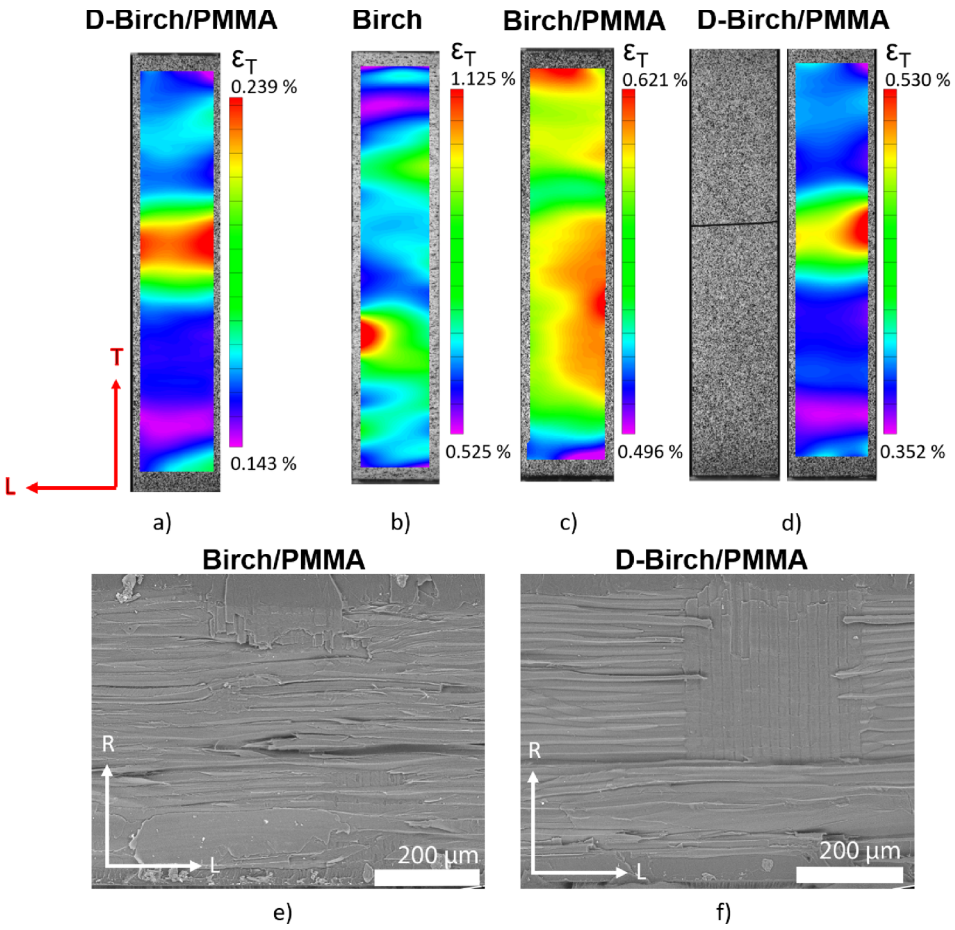

Fig. 6. Transverse strain fields for neat birch, Birch/PMMA and D-Birch/PMMA in the low strain region, at strains close to failure in transverse tension (T-direction is vertical), and SEM images of the fracture surfaces. Note that the color-coded strain-scales differ between different materials. (a) D-Birch/PMMA in low strain region; (b) neat birch; (c) Birch/PMMA; (d) D-Birch/PMMA with corresponding failed specimen; (e) Birch/PMMA with ray cells in the radial direction and fibers crossing over; (d) D-Birch/PMMA specimen with ray cells in the radial direction. (For interpretation of the references to colour in this figure legend, the reader is referred to the web version of this article.)

material axes as reference directions. For neat birch, the ε_{LT} strain field in Fig. 7(c), image to the far right, verifies that a region of strong shear deformation is obtained (note that magenta color-coded region has the highest strain), as intended with this off-axis test method. This is not so apparent for the corresponding strain field in Fig. 7(b) for the D-Birch/PMMA composite. The reason is the lower anisotropy in this material, see elastic constants in Table 2. Another observation from the strain fields in Fig. 7(b) is the multiaxial strain state in 10° off-axis specimens, in particular a substantial compressive transverse strain.

Strain fields for the two materials can be compared; and it is apparent from Fig. 7(b) and (c) that the porous birch reference again shows a much more inhomogeneous deformation field (note strain level scales are different for different strains and materials). Homogenization of strain fields in D-Birch/PMMA at the scale of fractions of millimeters is a consequence of the added polymer phase in the pore space of wood. This homogenization effect has not been emphasized previously, since local strain data are mostly lacking in the wood composites literature.

The shear strength, σ^*_{LT}, for D-Birch/PMMA was around 19 MPa, but only about 6 MPa for neat birch, most likely due to failure in local regions softened by cell wall bending. Both materials show fracture surfaces in the plane of the maximum shear stress direction, in support of shear failure. Absolute values of strength from off-axis shear testing, however, are not reliable due to shear coupling effects [27]. It is possible that local failure from deformation along the L-axis occurs for the composite in Fig. 7(b). The average local strain, ε_L, is indeed close to the strain to failure in longitudinal tension, see Fig. 4.

3.3.4. Effective modulus of birch reinforcement

The reinforcement effects in longitudinal direction of D-Birch/PMMA and Birch/PMMA are of interest for materials design purposes. Since the wood fiber direction is parallel to the loading direction, the analogy of a unidirectional fiber/polymer matrix composite was used.

A simple rule of mixtures model for longitudinal properties of unidirectional composites was adopted

$$E_L = v_f E_{fL} + (1 - v_f) E_m \tag{4}$$

In Eq. (4), E_{fL} denotes the effective elastic modulus of reinforcement material along the L-axis and data for volume fractions of reinforcement material, v_f, and elastic modulus of PMMA, E_m, are found in Table 2. As a consequence, the modulus of transparent wood scales with volume fractions and moduli of polymer and of wood cell wall material, according to Eq. (4). The axial properties of the cell wall material of birch was determined by the relationship for porous honeycombs loaded in the direction of the cell wall orientation [13]. This model has been used previously to analyze wood cell wall properties [13].

$$E_L = E_{fL}\left(\frac{\rho^*}{\rho_s}\right) = E_{fL} v_f \tag{5}$$

where E_{fL} is the effective elastic cell wall modulus along the L-axis and ρ* is the density of birch (data from Table 2) and ρ_s is the density of the cell wall (≈1500 kg/m^3). The effective elastic cell wall modulus, E_{fL}, for neat birch can be found by using Eq. (5), and data in Table 4. The result is $E_{fL} \approx 40$ GPa which is similar to a previous report [30], but slightly higher than the 35 GPa value suggested for wood species in general by Gibson and Ashby [31].

The measured E_L for Birch/PMMA is used in Eq. (4) with data from Table 4 in order to obtain an effective cell wall modulus for the biocomposite of $E_{fL} \approx 47$ GPa (effective modulus for neat birch reinforcement in Birch/PMMA). The increase in E_{fL} from 40 for neat birch to 47 GPa for the neat birch reinforcement in Birch/PMMA is interesting, since the modulus contribution from the cell wall is higher for Birch/PMMA. If confirmed by additional data, it possibly means that

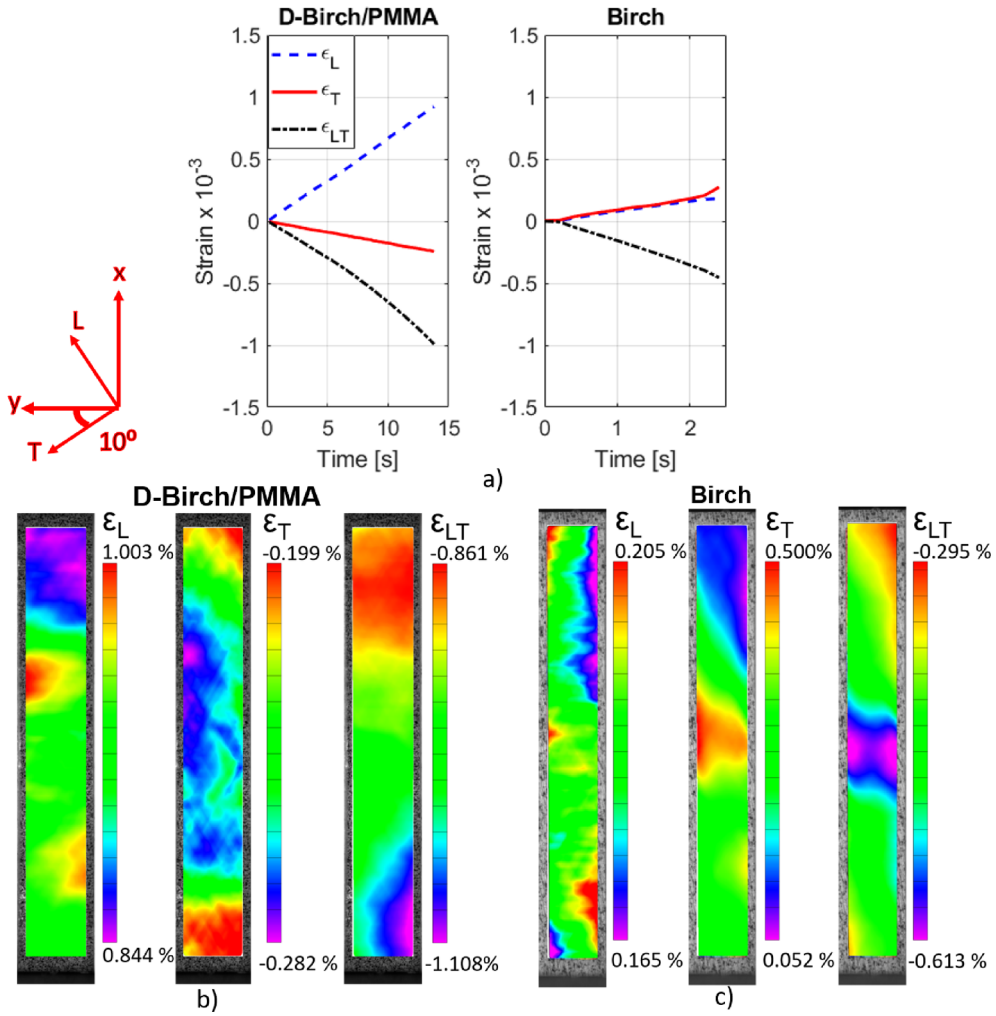

Fig. 7. Strain fields maps, for D-birch/PMMA and neat birch. Note that data are for material directions L, T and LT subjected to in-plane shear loading at high strain, close to failure. Fibers are inclined at 10° from the loading axis (vertical direction); (a) Average strains as a function of loading time for D-Birch/PMMA and neat birch; (b) Strain fields for D-Birch/PMMA; (c) Strain fields for neat birch. Note that color-coded strain scales are different for different materials and strains. (For interpretation of the references to colour in this figure legend, the reader is referred to the web version of this article.)

Table 4
Effective cell wall modulus estimated from rule of mixtures approaches (Eqs. (4) and (5)).

Material	E_{fL} [GPa]
D-Birch/PMMA	69.7
Birch/PMMA	46.8
Birch	39.9

the cell wall contribution is improved for polymer matrix composites, due to more efficient stress transfer when wood is embedded in a polymer matrix. In native wood, the inhomogeneity of the structure leads to locally inhomogeneous stress distribution, and this may lower the effective global stiffness.

For D-Birch/PMMA composites, the reinforcement effect from the cellulosic D-Birch phase is very strong, much stronger than for neat birch. The effective E_{fL} is as high as 69.7 GPa for the D-Birch phase. This is mainly due to the higher cellulose content in D-Birch (≈70% vs 50%), see Table 1. Again, a simple rule of mixtures approach would show that the increased cellulose content in D-Birch leads to increased modulus of the cell wall composite (oriented cellulose fibrils in a wood biopolymer matrix) since the volume fraction of the high modulus cellulose fibrils is increased. Delignification is therefore a useful method to improve the modulus of the reinforcement, despite the fact that the mechanical integrity of the delignified template by itself is poor, that it cannot even be subjected to mechanical testing. When the pore space in this fragile template is impregnated and polymerized to form a PMMA matrix phase, stress transfer is improved so that transparent D-Birch/PMMA reaches a modulus as high as 19 GPa at a volume fraction of only 25%, and the strength reaches 270 MPa.

3.3.5. *Effective ultimate strength of D-Birch*

The longitudinal strength of the delignified D-Birch template can be estimated from a rule of mixtures for strength

$$\sigma_L^* = \sigma_{fL}^* v_f + \sigma_m^s v_m \quad (6)$$

where σ_{fL}^* is the ultimate strength of D-Birch and σ_m^s is the stress in the matrix material at σ_L^*.The stress σ_m^s in PMMA is estimated from the strain ε_L^* for D-Birch/PMMA. Although the approach is simplistic, since real fracture mechanisms will be progressive and of significant complexity, the concept of effective strength is helpful in assessment of the strength reinforcement effects.

An effective wood template strength of around 960 MPa for σ_{fL}^* is estimated from Eq. (6) by using data for σ_L^*, v_f and v_m in Tables 2 and 3. This is dramatically higher than the effective wood tissue strength of 350 MPa reported by Gibson and Ashby [31], which is based on data for longitudinal strength for standardized specimens of a large number of wood species. Again, this indicates that the stress transfer in the present biocomposites is

highly favorable. The reason may be that small MMA monomers are able to fully impregnate the wood reinforcement template, forming a composite of low porosity and defect content. Local inhomogeneities in structure then function in a comparably homogeneous stress field, since the reinforcing wood template is embedded in polymer. A previous study on delignified single wood fibers indicates that individual fiber strength σ_{fL}^{*} can be as high as 1200 MPa for low microfibril angles [32]. This seems reasonable, since the probability for large defects is higher in a larger volume of material (veneer consisting of many fibers). It also lends some support to the present strength estimates for delignified veneer.

4. Conclusions

Delignified birch veneer provides unexpectedly strong reinforcement effects in transparent wood/PMMA biocomposites, despite the fragility of the neat delignified veneer. The values for effective cell wall modulus and effective cell wall strength are 70 GPa and 940 MPa, respectively. As a consequence, transparent wood reaches 19 GPa modulus and ultimate strength of 263 MPa at a wood template volume fraction of only 25%; and the optical transmittance is 70% at 1.3 mm thickness. This is in support of delignified veneer as a suitable eco-friendly and biobased reinforcement for multifunctional biocomposites based on wood nanotechnology. Improved eco-friendly characteristics could include the use of a biobased polymer and the development of a recycling protocol. High cellulose content, and favorable wood-polymer stress-transfer are important reasons for the reinforcement effects; and PMMA is well-distributed also at nanoscale due to the careful impregnation process by MMA monomers. For larger transparent wood structures, structural wood defects (e.g. fiber misalignment) and imperfect impregnation may lower the performance.

The DIC technique was successfully used to determine the elastic properties E_L, E_T, G_{LT} and ν_{LT} of "unidirectional" neat birch and transparent Birch/PMMA plies, by measuring the full strain field. Compared with neat birch, there was a very strong increase in E_T for the birch/PMMA composites so that the anisotropy ratio E_L/E_T was decreased. Cell wall bending mechanisms in native and porous wood were suppressed and replaced by Birch/PMMA composite stretching. Based on the elastic constants, plywood laminates can be designed for tailored stiffness properties.

Neat birch showed highly inhomogeneous strain fields, due to the anisotropic heterogeneity of the cellular structure, including annual rings of different local density. In contrast, D-Birch/PMMA and Birch/PMMA showed much more homogeneous strain-fields since locally soft regions were substantially stiffened by the PMMA polymer phase, with reduced local anisotropy. Damage mechanisms were interpreted during increased loading; and damage development was delayed for Birch/PMMA and D-Birch/PMMA composites. In transverse tension, failure was initiated by edge cracks. Strain-field measurements are well suited for interpretation of deformation and failure in wood and transparent wood composites, but it is important to avoid artefacts from the measurement technique. Because of challenging surface characteristics, local anisotropy and heterogeneity, improvements in speckle pattern, lighting and camera resolution are desirable. The choice of subset and step size also needs careful consideration in order to properly balance strain field resolution and measurement noise.

Acknowledgements

We acknowledge the funding from the European Research Council project No. 63636, Wood NanoTech. Xuan Yang is acknowledged for Klason Lignin, carbohydrate analysis and X-ray diffraction experiments, Hui Chen for transmittance and haze measurements. Professor Michel Grédiac from University of Clermont Auvergne is acknowledged for helpful suggestions with respect to the DIC analysis of existing data.

Declaration of Competing Interest

The authors declare no competing financial interest.

References

[1] Zhu M, Song J, Li T, Gong A, Wang Y, Dai J, et al. Highly anisotropic, highly transparent wood composites. Adv Mater 2016;28:5181–7.
[2] Li Y, Fu Q, Yu S, Yan M, Berglund L. Optically transparent wood from a nanoporous cellulosic template: combining functional and structural performance. Biomacromolecules 2016;17:1358–64.
[3] Lin H, Day DE, Stoffer JO. Optical and mechanical properties of optically transparent poly(methyl methacrylate) composites. Polym Eng Sci 1992;32:344–50.
[4] Fu Q, Yan M, Jungstedt E, Yang X, Li Y, Berglund LA. Transparent plywood as a load-bearing and luminescent biocomposite. Compos Sci Technol 2018;164:296–303.
[5] Bodig J, Jayne BA. Mechanics of wood and wood composites. Krieger; 1993.
[6] Dinwoodie JM. Timber: its nature and behaviour. 2nd ed. E & FN Spon; 2000.
[7] Grédiac M. The use of full-field measurement methods in composite material characterization: interest and limitations. Compos Part A 2004;35:751–61.
[8] Zink GA, Davidson RW, Hanna BR. Strain measurement in wood using a digital image correlation technique. Soc Wood Sci Technol 1995;27:346–59.
[9] Hochreiner G, Füssl J, Serrano E, Eberhardsteiner J. Influence of wooden board strength class on the performance of cross-laminated timber plates investigated by means of full-field deformation measurements. Strain 2014;50:161–73.
[10] Bjurhager I, Berglund LA, Bardage SL, Sundberg B. Mechanical characterization of juvenile European aspen (Populus tremula) and hybrid aspen (Populus tremula × Populus tremuloides) using full-field strain measurements. J Wood Sci 2008;54:349–55.
[11] Young G, Daniel J, Zink-Sharp A. Orthotropic properties of loblolly pine (Pinus taeda) strands. J Mater Sci 2010;45:5820–30.
[12] Hassel BI, Berard P, Modén CS, Berglund LA. The single cube apparatus for shear testing - full-field strain data and finite element analysis of wood in transverse shear. Compos Sci Technol 2009;69:877–82.
[13] Easterling KE, Harrysson R, Gibson LJ, Ashby MF. On the mechanics of balsa and other woods. Proc R Soc A Math Phys Eng Sci 2006;383:31–41.
[14] Ljungdahl J, Berglund LA, Burman M. Transverse anisotropy of compressive failure in European oak – a digital speckle photography study. Holzforschung 2006;60:190–5.
[15] Siau JF, Davidson RW, Meyer JA, Skaar C. A geometrical model for wood-polymer composites. Wood Sci 1968;1:116–28.
[16] Chamis CC, Sinclair JH. Ten-deg off-axis test for shear properties in fiber composites. Exp Mech 1977;17:339–46.
[17] TAPPI T 222 Om-02. Acid-insoluble lignin in wood and pulp. TAPPI Test Methods 2006:7.
[18] Willför S, Sundberg A, Pranovich A, Holmbom B. Polysaccharides in some industrially important hardwood species. Wood Sci Technol 2005;39:601–17.
[19] ASTM D1003-13. Standard Test Method for Haze and Luminous Transmittance of Transparent Plastics. ASTM Int; 2013:1–7.
[20] Sutton MA, Yan JH, Tiwari V, Schreier HW, Orteu JJ. The effect of out-of-plane motion on 2D and 3D digital image correlation measurements. Opt Lasers Eng 2008;46:746–57.
[21] Lecompte D, Smits A, Bossuyt S, Sol H, Vantomme J, Van Hemelrijck D, et al. Quality assessment of speckle patterns for digital image correlation. Opt Lasers Eng 2006;44:1132–45.
[22] Pagano NJ, Halpin JC. Influence of end constraint in the testing of anisotropic bodies. J Compos Mater 1968;2:18–31.
[23] Li Y, Fu Q, Rojas R, Yan M, Lawoko M, Berglund L. Lignin-retaining transparent wood. ChemSusChem 2017;10:3445–51.
[24] Preston RD. The organization of the cell wall of the conifer tracheid. Philos Trans R Soc, B 1934;224:131–74.
[25] Liu JY. Analysis of off-axis tension test of wood specimens. Wood Fiber Sci 2002;34:205–11.
[26] Modén CS. Micromechanics of softwoods in the transverse plane — effects on cell and annual ring scales. PhD Dissertation, KTH, TRITA-AVE; 2008:64, ISBN 9789174151817, 2008.
[27] Pindera MJ, Herakovich CT. Shear characterization of unidirectional composites with the off-axis tension test. Exp Mech 1986;26:103–12.
[28] Smith I, Landis E. Fracture and Fatigue in Wood. 1st ed. John Wiley & Sons Ltd; 2003.
[29] Cook J, Gordon JE. A mechanism for the control of crack propagation in all-brittle systems. Proc R Soc A Math Phys Eng Sci 1964;282:508–20.
[30] Cave ID. The longitudinal Young's modulus of Pinus radiata. Wood Sci Technol 1969;3:40–8.
[31] Gibson LJ, Wood Ashby MF. Cellular solids structure and properties. 2nd ed., Cambridge: Cambridge University Press; 1997. p. 387–428.
[32] Yang X, Berthold F, Berglund LA. Preserving cellulose structure: delignified wood fibers for paper structures of high strength and transparency. Biomacromolecules 2018;19:3020–9.